Numerical analysis of static and dynamic wind turbine airfoil characteristics in transonic flow

Vitulano, M. C.; De Tavernier, D.; De Stefano, G.; Von Terzi, D.

DOI
10.1088/1742-6596/2767/2/022013

Publication date
2024

Document Version
Final published version

Published in
Journal of Physics: Conference Series

Numerical analysis of static and dynamic wind turbine airfoil characteristics in transonic flow

Journal of Physics: Conference Series **2767** (2024) 022013 doi:10.1088/1742-6596/2767/2/022013

Numerical analysis of static and dynamic wind turbine airfoil characteristics in transonic flow

M C Vitulano[1,2], D De Tavernier[2], G De Stefano[1] and D von Terzi[2]

[1] **Engineering Department, University of Campania Luigi Vanvitelli, 81031 Aversa, Italy**

[2] **Aerospace Engineering Faculty, Delft University of Technology, 2629HS Delft, The Netherlands**

E-mail: m.c.vitulano@tudelft.nl

Abstract.

This study performed an aerodynamic characterization of the FFA-W3-211 wind turbine tip airfoil in transonic flow using Unsteady Reynolds-Averaged Navier-Stokes (URANS) simulations, for both steady and dynamic operational conditions. First, the boundary between subsonic and supersonic flow in static conditions was identified, depending on the angle of attack, the approach flow Mach number, and the Reynolds number. The analysis points out that higher Reynolds numbers promote the occurrence of local supersonic flow. Thereafter, to investigate the dynamic behavior in the transonic flow regime, a sinusoidal pitching motion with representative values was imposed. A hysteresis, similar to but distinct from dynamic stall, was observed for entering and leaving the supersonic and subsonic regions. Elevated reduced frequencies widened the hysteresis loop, resulting in increased normal forces on the airfoil. The study indicated that an increase in reduced frequency leads to an earlier onset of transonic flow. In conclusion, the risk of transonic flow occurring during normal operation of the next generation wind turbines predicted in earlier studies could be corroborated. Moreover, dynamic effects and Reynolds number dependencies can be significant.

1. Introduction

Wind turbine blades have grown in size, with the largest ones exceeding the length of 100 meters. This results in higher tip speeds, both for current and next-generation wind turbines, approaching 100 m/s and possibly beyond. In these operational conditions, wind turbine blades face airflows with inflow Mach number up to 0.3, potentially violating the assumption of incompressibility, and leading to local supersonic flow at the outboard airfoils. Therefore, understanding the aerodynamics of compressible and, in particular, transonic flow is crucial in designing the next generation of wind turbines and assessing risks related to performance, loading, and fatigue.

Several academic efforts have been focused on exploring the effects of high-speed flows on large rotors. The EU AVATAR (AdVanced Aerodynamic Tools of lArge Rotors) project aimed to improve and validate aerodynamic models, and to ensure their applicability for large wind turbines rotors (with a power of 10MW and larger), using wind tunnel tests and CFD simulations [1]. As part of this project, Sørensen et al. [2] carried out a two-dimensional airfoil investigation on the effects of compressibility in the tip region of large wind turbines of 20 MW size. This analysis suggests that incompressibility assumptions might be violated in the

tip region of the turbine blades. They also show that compressibility corrections are insufficient outside the linear region of the lift curve, where a full compressible formulation should be applied. Some authors suggest that neglecting compressibility effects could lead to a mismatch between the estimated rotor power and the one effectively produced [3, 4, 5]. Recently, Cao et al. [6] conducted a comparative study on the aerodynamic performances of the IEA-15MW offshore reference wind turbine (RWT) under both compressible and incompressible conditions. Their results confirm that the compressible flow simulation estimates an higher thrust value by 1.4% compared to the incompressible one, while the torque is nearly 11% higher. Mezzacapo et al. [7] also performed a similar analysis on the compressible aerodynamics of the IEA-15MW RWT employing URANS computations. This study suggests that URANS can help in understanding the aerodynamic features of the wind turbine blade in the compressible regime.

While earlier research recognized the potential impact of compressibility on large wind turbines due to density variations, it was only very recently that De Tavernier and von Terzi [8] demonstrated that the next-generation wind turbines could face transonic flow. They analyzed the operational condition of the IEA-15MW RWT using the software OpenFast and compressibility corrections for the airfoil polars. Considering angle of attack changes due to inflow turbulence, their study revealed that, near the cut-out wind speed, local supersonic flow can appear on a portion of the tip airfoils. In such conditions, the blade is operating at large negative angles of attack and the flow is significantly more accelerated over the airfoil nose. Moreover, transonic flow could potentially occur even at lower wind speeds in off-design conditions. Recently, these results have been validated experimentally by [9].

The approach presented in [8] allows to identify where and when transonic flow might occur when operating a wind turbine. Nevertheless, there are uncertainties in the results due to the application of compressibility corrections on airfoil polars, as previously indicated by [2]. In addition, this approach becomes invalid once transonic flow indeed occurs.

In fact, a knowledge gap exists regarding the behavior of wind turbines blade airfoils in transonic flow conditions. Only Hossain et al. [10] investigated the propagation of shocks on the NREL Phase VI S809 airfoil by means of URANS. However, they considered only positive angles of attack at an inflow Mach number of 0.8, which is still very far from what wind turbines encounter. It is important to note that, if transonic flow is going to appear, shocks, flow separation and buffetting can be expected representing a significant risk related to performance, loads, and fatigue-life predictions of affected wind turbine rotors.

It is also important to underline that wind turbines are affected by complicated environmental phenomena, such as atmospheric turbulence, ground boundary layer effects, directional and spatial variations in wind shear, thermal stratification, and the possible effects of an upstream unsteady wake, which lead the blade section to operates in unsteady aerodynamic conditions [11]. These unsteadiness sources can be represented as periodic and aperiodic contributions, which are affected by compressibility and transonic effects [12].

The aim of the present work is to investigate how transonic flow affects the FFA-W3-211 wind turbine airfoil that is used at the blade tip of the IEA 15MW RWT [13] (and its announced successor the 22MW RWT). There are two main objectives: (1) to establish the limit for which transonic flow can occur for steady operating conditions, and (2) to characterize the dynamic flow behavior when entering and leaving the supersonic and subsonic regimes.

2. Methodology

2.1. Numerical set-up

All simulations are performed using the open-source software OpenFoam, employing the transient solver rhoPimpleFoam, for turbulent compressible flow regimes [14]. A fully turbulent flow is considered in the present work, using the k-ω Shear Stress Transport (SST) model [15] to take into account turbulence effects on the resolved mean flow. Free-stream boundary conditions

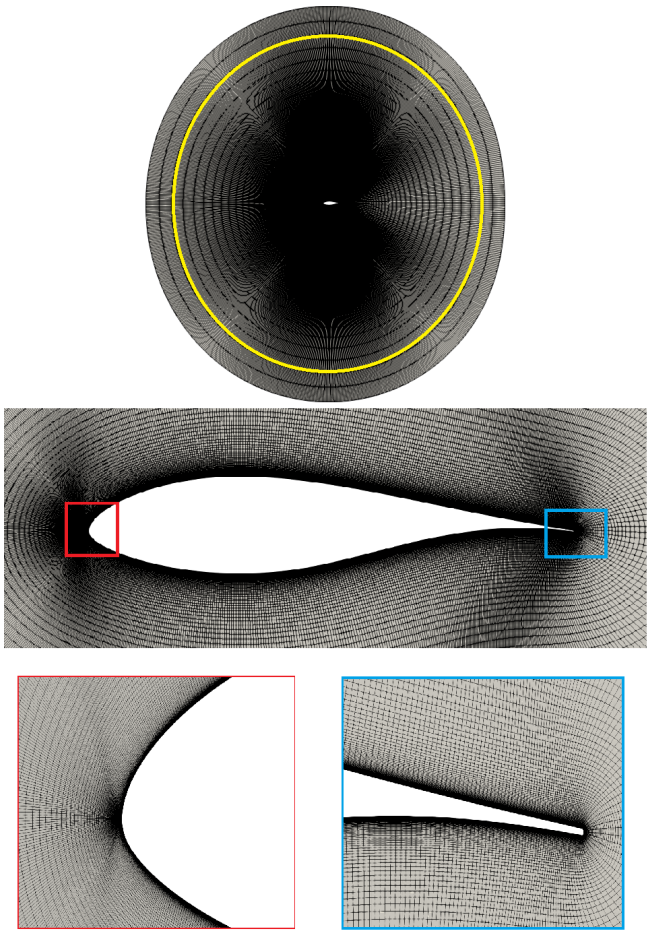

Figure 1. Sketch of the computational domain (top), the FFA-W3-211 wind turbine airfoil (middle), and details of the leading and trailing edges (bottom).

are applied to pressure, velocity, and temperature fields. At the wall, no-slip boundary conditions are imposed, and wall functions are used to model the near-wall region. Spatial variables are discretized using a second-order scheme, while the first-order implicit Euler scheme is used for the time integration. A maximum Courant number of 0.5 is prescribed to ensure temporal accuracy and numerical stability. The numerical setup has been extensively discussed and validated in previous work [16].

In the first part of this study, the combination of angle of attack and inflow Mach number for critical conditions is determined, i.e. the boundary between subsonic and supersonic flow regimes is established. Fixing the inflow Mach number, the minimum pressure coefficient is evaluated for several angles of attack, obtaining an array of discrete values as $[(C_{p_{\min,1}},\alpha_1), ..., (C_{p_{\min,n}},\alpha_n)]$. Then, these points are interpolated to asses a continuous law that relates the minimum pressure peak and the angle of attack. Finally, the pressure suction peak is compared to the critical value at which the flow over the airfoil is locally attaining a supersonic flow, expressed as:

$$C_{p_{\text{crit}}} = \frac{2}{\gamma M_\infty^2} \cdot \left(\left[\frac{1 + \frac{1}{2}(\gamma - 1) M_\infty^2}{1 + \frac{1}{2}(\gamma - 1) M_{crit}^2} \right]^{\frac{\gamma}{\gamma - 1}} - 1 \right) \tag{1}$$

The angle of attack corresponding to the conditions for which the suction peak reaches the

critical value is defined as the critical angle of attack, for that specific inflow Mach number.

To assess the appropriateness of this procedure, a comparison with data obtained by means of a compressible correction is performed. The suction peak for a fixed angle of attack is calculated using the software Xfoil [17], in the incompressible regime. This value is adapted as function of the Mach number using the following Prandtl-Glauert compressibility correction:

$$C_{p_c} = \frac{C_{p_i}}{\sqrt{1 - M_\infty^2}} \tag{2}$$

This way, the inflow Mach number according to which Equations (1) and (2) provide the same value corresponds to the critical Mach number for a fixed angle of attack.

In the present study, a dynamic pitching motion of the airfoil is also considered. For this purpose, the computational domain, which is shown in Figure 1, is divided into two regions composed of two concentric circles, whose inner one contains the airfoil. The outer circle is fixed respect to the reference system, while the inner one oscillates together with the airfoil. The interface between the two circles (represented in yellow in Figure 1) is handled by the cyclic Arbitrary Mesh Interface (AMI). The cyclic AMI algorithm deals with periodic interface which discretization is equivalent to connect two adjacent blocks which can have also non-conforming faces and can be even cyclic. This approach ensures a high convergence rate and the robustness of the simulations [18].

2.2. Case study

The present work focuses on the aerodynamic behaviour of the blade tip of the IEA-15MW RWT. This turbine is strategically engineered using industry input to play a significant role in driving the ongoing evolution of next-generation wind turbine technologies. A recent study shows the potential occurrence of transonic flow under normal operational conditions, especially at cut-out wind speed, when the blade is pitched to large negative angles of attack, with shedding power in excess of rated conditions of the generator [8]. As the wind speed increases beyond rated wind speed, the blades adjust their pitch in order to maintain a rated power. [8], showed that close to cut out wind speed, the blades of the IEA 15WM reached high negative angles of attack. Figure 2 shows the operational conditions, in terms of inflow Mach number and angle of attack, in which transonic flow can occur for a given wind speed. Each blue dot represents the turbine operating conditions for a given time-step of an unsteady OpenFAST simulation with inflow turbulence. The case shown in the figure shows some points crossing the predicted supersonic boundary.

Two sets of simulations are conducted. The first set serves to establish the transonic flow threshold using URANS. This analysis is carried out for pairs of angles of attack and Mach numbers in the vicinity of the conditions where transonic flow was predicted in [8], as shown in Figure 2. Two Reynolds numbers are considered: 1.8 and 9 million. The former one is a value for which wind tunnel measurements for this airfoil exist. It is also in the order of values typically used to determine experimentally airfoil polars for wind turbine applications. The second value is the Reynolds number at which the airfoil would be operated for the full-scale wind turbine. The second set of simulations involves a prescribed airfoil pitching motion across the threshold. The pitching mean and boundary values are indicates by the red crosses in Figure 2. The effective angle of attack is described in Equation 3, where the oscillation's mean geometric angle of attack is $a_m = -10^\circ$ and the amplitude is $a_0 = 5^\circ$. These values are in the operating range shown in Figure 2.

$$a_e(t) = a_m + a_0 \sin\left(\frac{2kt}{t_c}\right) \tag{3}$$

In Figure 3, the effective angle of attack for one period of oscillation is shown, as a function of the phase angle $\phi = 2kt/t_c$, where $t_c = c/U_\infty$ is the characteristic time-scale. In this figure, also

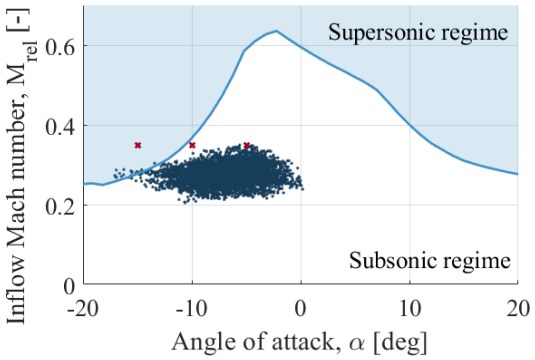

Figure 2. Operational conditions of the IEA-15MW RWT at r/R=0.97 (blue dots), the border of the supersonic flow regimes (blue line) from [8], and the pitching motion mean and boundary values (red crosses).

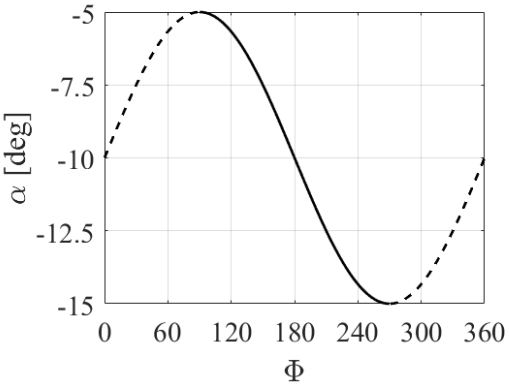

Figure 3. Evolution of the effective angle of attack during one period of oscillation for the pitching airfoil: downstroke (solid line) and upstroke (dashed line).

downstroke and upstroke are highlight, with the downstroke reffering to the pitching motion in which the airfoil advances into transonic flow, and the upstroke involving the motion where the airfoil moves out of the transonic flow. Note that the most important parameter governing the unsteady nature of the pitching motion is the reduced frequency $k = \pi f c/U_\infty$, where f is the physical frequency, c is the chord of the airfoil and U_∞ is the free-stream velocity. The present study is focused on an highly unsteady regime, considering $k > 0.2$ as found in [12], as reported in Table 1.

Table 1. Flow conditions for the dynamic simulations.

k	$f[Hz]$	$\omega[rad/s]$	M_∞	Re
0.4	15.3	96.1		
0.5	19.2	120.1	0.35	9×10^6
0.6	22.9	144.1		

3. Results

3.1. Static behaviour

Figure 4 summarizes a key result of the present work. This figure shows lines with a critical combination of angles of attack and inflow Mach numbers above which local supersonic flow on the FFA-W3-211 tip airfoil is observed. Results from URANS and Xfoil using the Prandtl-Glauert compressibility correction, both for fully turbulent flow, are shown for two different Reynolds numbers. For the same Mach number, the URANS predicts the appearance of transonic flow already for slightly smaller angles of attack. That is, for the more likely scenario, where the wind turbine is operated above rated wind speed (with negative angles of attack), the URANS suggests a larger area of safety, whereas the inverse would be true if the turbine were operated below rated wind speed (with positive angles of attack). Moreover, this analysis points out that, for both URANS and Xfoil, an increase in the Reynolds number promotes transition to

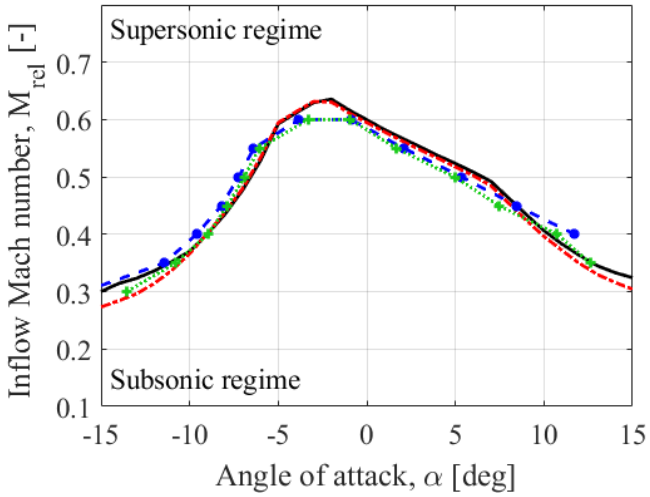

Figure 4. Subsonic-supersonic boundary for the FFA-W3-211 wind turbine tip airfoil: Xfoil Re=1.8×10^6 (black line), Xfoil Re=9×10^6 (red line), OpenFoam Re=1.8×10^6 (blue line) and OpenFoam Re=9×10^6 (green line).

a local supersonic flow, especially for larger (either negative or positive) angles of attack. As a consequence, typical wind tunnel studies that would likely be at lower Reynolds numbers than what the wind turbine operates in may be less conservative in any safety zone prediction.

Although the two techniques mostly show a good agreement, there are some discrepancies. In particular, this happens at the peak for Mach 0.6, due to a lack of data analyzed in the present work and for angles of attack above 12°, for Re=1.8×10^6. The latter mismatch resides in the post-stall region as demonstrated by [19], where both Xfoil and URANS results are less trustworthy. However, both operational conditions are quite far from those seen by wind turbines that would be at risk for transonic flow.

The curves shown in Figure 4 are obtained with pressure data and Equation (1). This corresponds to a suction peak crossing the red horizontal line in Figure 5(c). For the inflow Mach number of 0.35 shown in Figure 5, the static critical angle of attack for which transonic flow occurs has been found to be $-10.8°$, suggesting that transonic flow should only be discerned for $\alpha = -15°$, but not for $-10°$ and $-5°$ in this figure. This is confirmed by showing the presence of the supersonic pocket close to the leading edge in Figure 5(a) and a discontinuity in the density gradients contour maps in Figure 5(b) only for $\alpha = -15°$. This corroborates the fact that the analysis with the minimum pressure is viable for predicting supersonic flow on the airfoil, and provides credibility to the transonic flow risk predictions of the IEA-15MW RWT in [8].

3.2. Dynamic behaviour

Unsteadiness, and the associated change in the effective angle of attack, was crucial in identifying the occurrence of transonic flow on wind turbine tip airfoils in the present work, as in [8]. From dynamic stall, it is known that a hysteresis occurs for certain frequencies of unsteadiness. For example, one can see [20] and references therein. Here, the aim is to explore if a similar effect occurs for entering and leaving the supersonic flow regime in a wind turbine application, as identified in the previous section. To this end, it is assessed how a prescribed dynamic pitching motion in an highly unsteady regime can affect the transonic boundary.

Figure 6 shows the minimum pressure coefficient as function of the effective angle of attack.

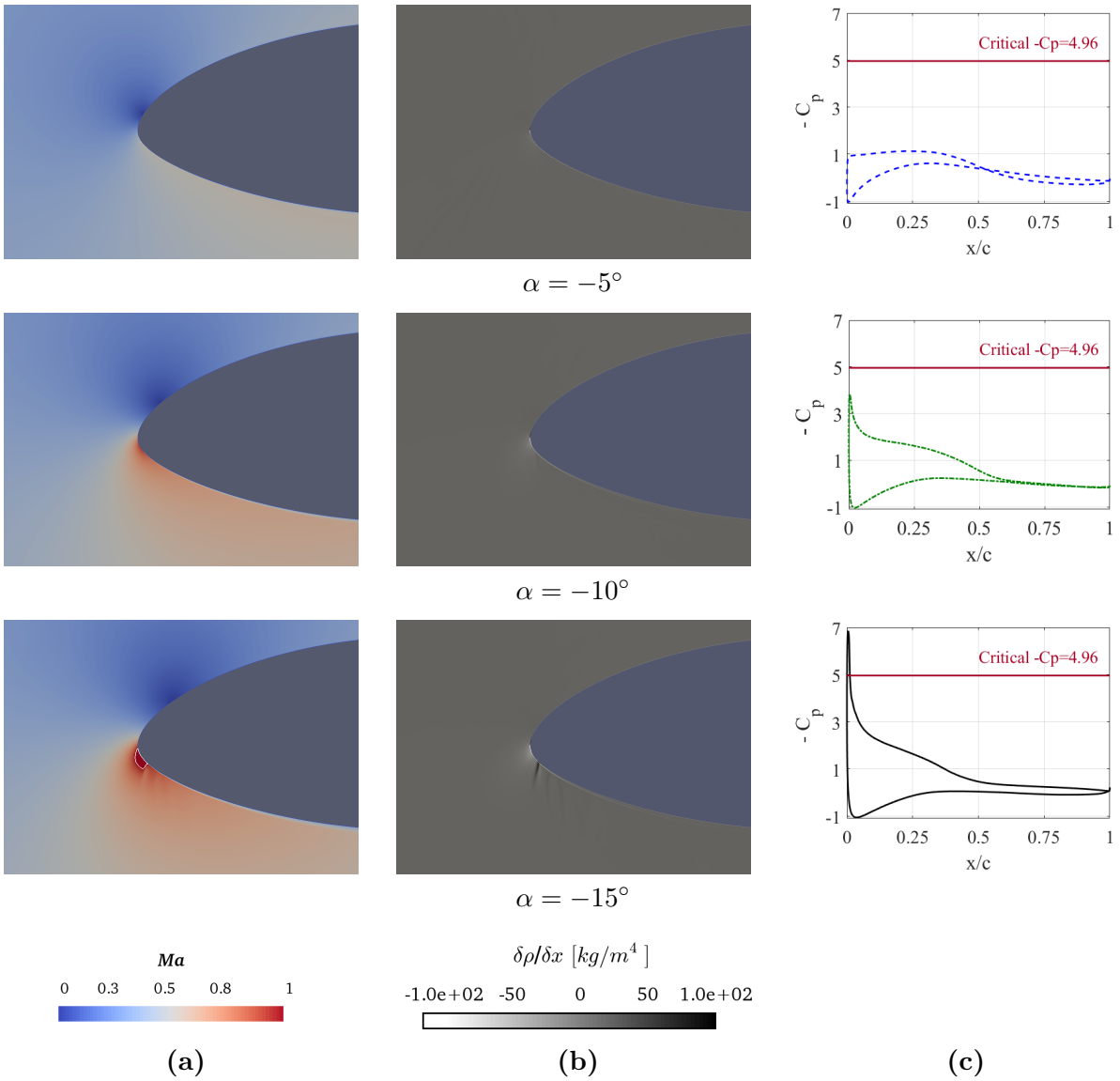

Figure 5. Contour maps of (a) Mach number with iso-contour at M=0.99, (b) Schlieren images and (c) mean pressure coefficient distribution; M_∞=0.35 and Re=9×10^6.

A marked hysteresis loop is established, with a clear dependence on the reduced frequency. This investigation reveals that an increase of the reduced frequency corresponds to an expanded array of configurations, in terms of angle of attack, where the maximum suction peak surpasses the critical threshold in Figure 6. In particular, considering the downstroke, transonic flow occurs later at $\alpha = -14.02°$ for k=0.4, $\alpha = -14.25°$ for k=0.5, and $\alpha = -14.36°$ for k=0.6 while in the static case, the critical angle of attack is equal to $-10.8°$, as shown by the yellow line. For the upstroke, instead, a delay is also shown, with the transonic flow that disappears later at $\alpha = -9.93°$ for k=0.4, $\alpha = -9.72°$ for k=0.5, and $\alpha = -9.39°$ for k=0.6. This implies that, as the reduced frequency increases, the transonic regime expands.

This delay is shown in Figure 7, where the contour maps of the Mach number for the upstroke and dowstroke are compared with the static case, for a fixed reduced frequency. At $\alpha = -10°$, transonic flow occurs only for the upstroke.

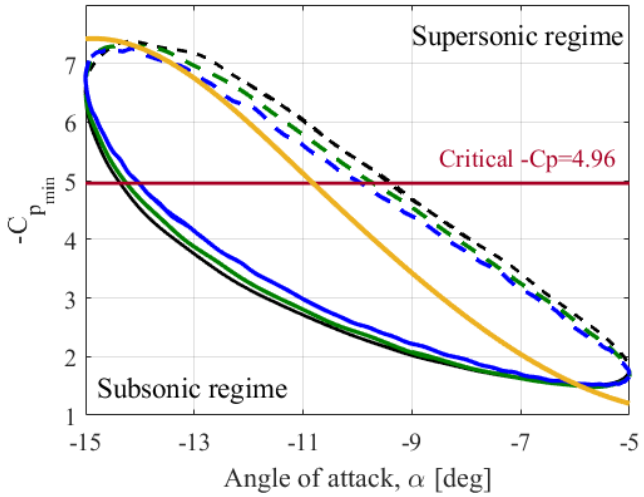

Figure 6. Minimum pressure coefficient as function of the effective angle of attack for k=0.4 (blue line), k=0.5 (green line), k=0.6 (black line), k=0 (yellow line); M_∞=0.35 and Re=9×10^6: downstroke (solid line), upstroke (dashed line).

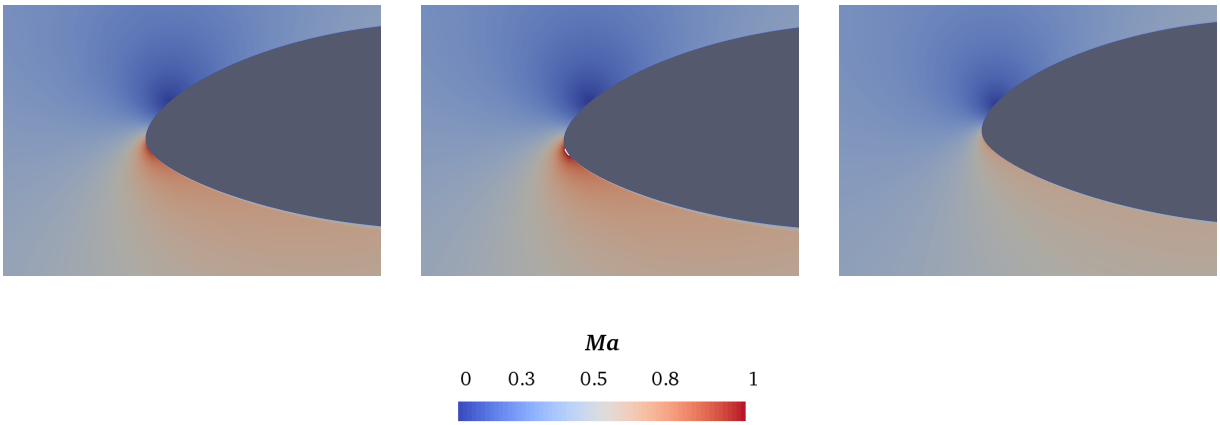

Figure 7. Contour maps of Mach number with iso-contour at M=0.99, (a) k=0 (b) k=0.5 upstroke (c) k=0.5 downstroke; $\alpha = -10°$, M_∞=0.35 and Re=9×10^6.

Lift and drag coefficient curves, as function of the effective angle of attack, are presented in Figure 8 and Figure 9. Moderate hysteresis of lift coefficient can be seen, whereas hysteresis of the drag coefficient is more pronounced. Moreover, an increase in the reduced frequency is correlated to an expanded hysteresis loop for both lift and drag coefficients. This leads to a general increase of the normal force on the airfoil, as also proven experimentally by [21], with a resulting increment of both torque and thrust contributions.

4. Conclusions

In present work, the steady and (highly) unsteady aerodynamic characterization of the FFA-W3-211 wind turbine tip airfoil in transonic flow was performed. URANS simulations were carried out by means of a numerical setup already validated in [16], while employing a dynamic mesh

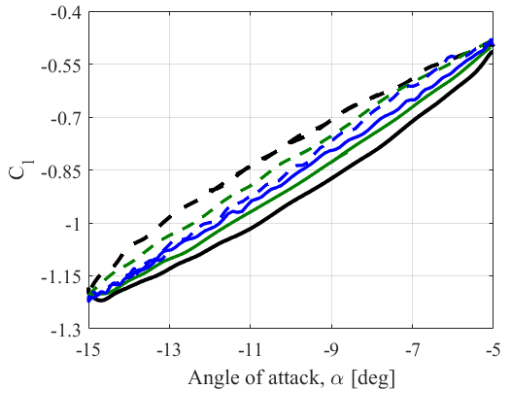

Figure 8. Lift coefficient as function of the effective angle of attack for k=0.4 (blue line), k=0.5 (green line), and k=0.6 (black line); M_∞=0.35 and Re=9×10^6: downstroke (solid line), upstroke (dashed line).

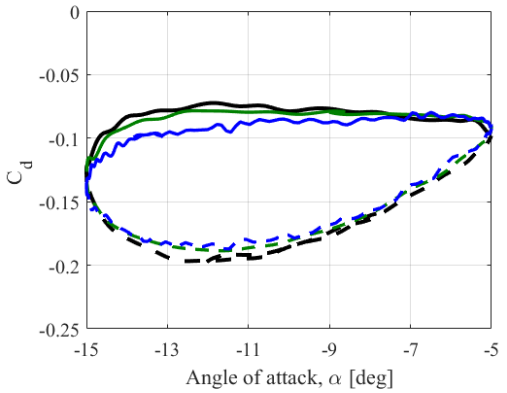

Figure 9. Drag coefficient as function of the effective angle of attack for k=0.4 (blue line), k=0.5 (green line), and k=0.6 (black line); M_∞=0.35 and Re=9×10^6: downstroke (solid line), upstroke (dashed line).

in order to introduce a sinusoidal pitching motion of the airfoil at different reduced frequencies.

In the first part of this work, the boundary between subsonic and supersonic flow in static operating conditions was identified and compared to results obtained by applying the Prandtl-Glauert compressibility correction. The two different approaches show similar results. A dependence on the Reynolds number was observed, especially for high (both positive and negative) angles of attack. The present analysis points out that an increase in the Reynolds number promotes the onset of local supersonic flow.

In the second part of the present study, the dynamic behavior of the airfoil when entering and leaving the supersonic flow regime was investigated. To this end, a sinusoidal pitching motion with characteristic frequencies below unity were introduced. A hysteresis, similar to but distinct from dynamic stall, was observed for entering and leaving the supersonic and subsonic regions. As a consequence, a hysteresis loop was also found for both lift and drag coefficients. Thereby, higher reduced frequencies resulted in an expanded hysteresis loop for both coefficients, leading to an increased normal force on the airfoil. A delay in transonic effects during both upstroke and downstroke in pitching motions is found. The present study also reveals that an increase of the reduced frequency leads to an increase in the number of configurations for which a transonic regime is established.

The presence of supersonic flow prompts new crucial research questions, concerning the influence of shock waves and buffeting on wind turbine performance and lifetime. A comprehensive evaluation of these effects is crucial to ensure the efficient operation and durability of next-generation large wind turbines. Given the highly unsteady and 3D nature of the phenomenon and the necessity to predict dominant frequencies for assessing aeroelastic instabilities, it becomes imperative to conduct experiments and/or high-fidelity numerical simulations. In this context, while frequently applied in aerospace research of transonic flows, it is prudent to consider the limitations of URANS in accurately capturing relevant flow phenomena due to how turbulence and the dynamics associated with shocks are modeled. In particular, URANS inherently diminishes a significant amount of relevant unsteadiness, redirecting the dominant frequency towards lower values [22]. It is also important to point out that this study considered only fully turbulent flow conditions, while transition phenomena may occur on clean wind turbine airfoils. Recognizing these limitations of the URANS approach, we propose the

adoption of a hybrid RANS/LES approach for further research (see [22] for a review). One example considered is the wall-modeled hybrid RANS/LES used in [23].

References

[1] Ceyhan JGSO, Boorsma K, Gonzalez A, Munduate X, Pires O, Sørensen N, Ferreira C, Sieros G, Madsen J, Voutsinas S, Lutz T, Barakos G, Colonia S, Heißelmann H, Meng F and Croce A 2016 Latest results from the EU project AVATAR: Aerodynamic modelling of 10 MW wind turbines *J. Phys.: Conf. Ser.* **753** 022047

[2] Sørensen NN, Bertagnolio F, Jost E and Lutz T 2018 Aerodynamic effects of compressibility for wind turbines at high tip speeds *J. Phys.: Conf. Ser.* **1037** 022003

[3] Campobasso MS, Sanvito AG, Drofelnik J, Jackson A, Zhou Y, Xiao Q and Croce A 2018 Compressible Navier-Stokes analysis of floating wind turbine rotor aerodynamics *Int. Conf. on Offshore Mechanics and Arctic Engineering* **51975** V001T01A031

[4] Ortolani A, Persico G, Drofelnik J, Jackson A and Campobasso MS 2020 Cross-comparative analysis of loads and power of pitching floating offshore wind turbine rotors using frequency-domain Navier-Stokes CFD and blade element momentum theory *J. Phys.: Conf. Ser.* **1618** 052016

[5] Yan C and Archer CL 2018 Assessing compressibility effects on the performance of large horizontal-axis wind turbines *Appl. Energy* **212** 33-45

[6] Cao J, Qin Z, Ju Y, Chen Y, Shen WZ, Shen X and Ke S 2023 Study of air compressibility effects on the aerodynamic performance of the IEA-15 MW offshore wind turbine *Energy Convers. Manag.* **282** 116883

[7] Mezzacapo A, Vitulano MC, Tomasso AD and De Stefano G 2023 CFD prediction of wind turbine blade compressible aerodynamics, in: Proceedings of 23rd Int. Conf. on Computational Science and Its Applications *Lecture Notes in Computer Science* LNCS **13956** 113-125

[8] De Tavernier D and von Terzi D 2022 The emergence of supersonic flow on wind turbines *J. Phys.: Conf. Ser.* **2265** 042068

[9] Aditya A, De Tavernier D, Schrijer F, van Oudheusden B and von Terzi D 2024 Experimental investigation of the occurrence of transonic flow effects on the FFA-W3-211 airfoil *J. Phys.: Conf. Ser.* (submitted)

[10] Hossain MA, Huque Z and Kammalapati RR 2013 Propagation of shock on NREL phase VI wind turbine airfoil under compressible flow *J. Renew. Energy* **2265** 042068

[11] Leishman JG 2002 Challenges in modelling the unsteady aerodynamics of wind turbines *Wind Energy* **5** 85-132

[12] Corke TC and Thomas FO 2015 Dynamic stall in pitching airfoils: aerodynamic damping and compressibility effects *Annu. Rev. Fluid Mech.* **47** 479-505

[13] Gaertner E, Rinker J, Sethuraman L, Zahle F, Anderson B, Barter G, Abbas N, Meng, F, Bortolotti P, Skrzypinski W, Scott G, Feil R, Bredmose H, Dykens K, Shields M, Allen C and Viselli A 2020 IEA wind TCP task 37: definition of the IEA 15-megawatt offshore reference wind turbine *National Renewable Energy Laboratory*

[14] OpenFOAM Foundation 2016 *OpenFOAM User's Guide* Version 4.1

[15] Menter FR 1994 Two-equation eddy-viscosity turbulence models for engineering applications *AIAA J.* **32** 1598–1605

[16] Vitulano MC, De Tavernier D, De Stefano G and von Terzi D 2023 Numerical analysis of transonic flow over the FFA-W3-211 wind turbine tip airfoil *14th International ERCOFTAC Symposium on Engineering Turbulence Modelling and Measurements, Barcelona, Spain 6-8 September 2023*

[17] Drela M and Youngren H 2001 *XFOIL 6.94 User Guide*

[18] Mangani L, Buchmayr M, Darwish M and Moukalled F 2017 A fully coupled OpenFOAM® solver for transient incompressible turbulent flows in ALE formulation *Numer. Heat Tr. B-Fund.* **71** 313-326

[19] Bertagnolio F, Sørensen N, Johansen J and Fuglsang P 2001 *Wind Turbine Airfoil Catalogue*

[20] Chellini S, De Tavernier D and von Terzi D 2024 Impact of dynamic stall model tailoring on wind turbine loads and performance prediction *J. Phys.: Conf. Ser.* (submitted)

[21] Chellini S, De Tavernier D and von Terzi D 2023 Experimental characterization of unsteady airfoil aerodynamics for wind turbine applications *14th International ERCOFTAC Symposium on Engineering Turbulence Modelling and Measurements, Barcelona, Spain 6-8 September 2023*

[22] Fröhlich J and von Terzi D 2008 Hybrid LES/RANS methods for the simulation of turbulent flows *J. Prog. Aerosp. Sci.* **44** 349-377

[23] Salomone T, Piomelli U and De Stefano G 2023 Wall-modeled and hybrid large-eddy simulations of the flow over roughness strips *Fluids* **8** 10